The Astrophysical Journal, 360: 343–351, 1990 September 10

A SIMPLE MODEL FOR DISSIPATIVE GALAXY FORMATION

Mario G. Abadi,[1] Diego García Lambas, and Mirta B. Mosconi
Observatorio Astronómico, Universidad Nacional de Córdoba, Argentina
Received 1989 January 3; accepted 1990 February 22

ABSTRACT

Numerical experiments of the dynamics of a distribution of interacting gas clouds in a protogalactic potential well are analyzed. Dissipation of energy by means of inelastic cloud-cloud collisions produce, after a few characteristic times, a strong flattening (5:1), and a large ratio of rotational versus total kinetic energy for the clouds with several inelastic collisions.

The adimensional spin parameter $\lambda = J|E|^{1/2}G^{-1}M^{-5/2}$ reaches high values ($\lambda \geq 0.25$) for this highly dissipative component, in contrast with $\lambda \simeq 0.07$, for those clouds that never collided.

After the collapse, the resulting systems live in a "long" stationary state, where the collisions gradually increase the number of "star clusters," made up of gas clouds with a threshold condition in the number of inelastic collisions.

Gasdynamical effects involving energy dissipation and relaxation processes play fundamental roles in the galaxy formation model depicted here. We conclude from our experiments that accretion from a gaseous medium surrounding a galactic potential well can account for many desirable properties of a model of disk galaxy formation.

Subject headings: galaxies: formation — galaxies: structure

I. INTRODUCTION

Many accepted modern theories of the origin of structures in the universe assume that present observed inhomogeneities have evolved out of a primordial Gaussian density perturbation field (Peebles 1980; Efstathiou and Silk 1983). In this canonical cosmology, one expects to find a statistical distribution of the angular momentum of bound objects. This distribution is of great importance in a bottom-up scenario, in particular for the biased models (Davis *et al.* 1985), in which 1 σ perturbations might end up in objects associated with disk galaxies.

Some galaxy models (Caldwell and Ostriker 1982; Bahcall, Schmidt, and Soneira 1982; Blumenthal *et al.* 1986; Carlberg 1988*a*, *b*) distinguish between dissipative and nondissipative components; other models consider a dissipationless rigid halo of dark material for the dissipative component (Fall and Efstathiou 1980).

The amount of rotation is conveniently expressed in terms of the adimensional spin parameter λ (Peebles 1969). In the gravitational instability picture, the dominant perturbations at recombination are in subgalactic mass scales. These perturbations grew and formed a hierarchy of structures that acquired angular momentum from the tidal field produced by the neighboring mass distribution. The mean value for the spin parameter is $\lambda \simeq 0.07$ (Peebles 1969; Efstathiou and Jones 1979).

In a biased galaxy formation scheme, and for different primordial Gaussian fluctuation spectrums, a 1–2 σ deviation from the mean density in a window of a galaxy size has λ close to the original estimate around 0.07 (Hoffman 1988*a*, *b*).

Pioneering studies on the formation of disk galaxies including dissipation of energy (Sandage, Freeman, and Stokes 1970; Gott and Thuan 1976; Larson 1974, 1976) were able to account for several properties of flattened galaxies. Dissipation is generally considered to be a dominant process in the formation of disk galaxies, although it might also be important in the formation of ellipticals (Carlberg 1988*a*, *b*).

We concentrate here on the formation of strongly flattened structures. We consider the collapse of a distribution of dissipative gas clouds under the gravitational field of a dominant potential well. The dissipative component that has undergone several collisions tends to settle in a flattened, rotation-dominated structure. These rotationally supported structures are disks or rings in different experiments. They have a large fraction (20%–80%) of the total mass in clouds and are very stable along several crossing times.

The models include the dynamical influence of a massive halo of different masses. These halos represent either a primordial density enhancement where the galaxy forms or an already formed galactic potential well in which the gas of the new generation of stars is accreted.

The methods and initial conditions of the simulations are discussed in §§ II and III. Section IV outlines the dissipation scheme, § V analyzes the experiments, and finally in § VI we present a discussion of the main results.

II. MODELS

The models are based on the assumption that in early epochs, clumps of matter (dissipative or nondissipative) have piled in protogalactic halos, and large amounts of gas surrounding the growing protogalaxy remain in a cooling and fragmenting phase. When the gaseous component is sufficiently cold and pressure is negligible, the system of clouds tends to collapse, and the number of interpenetrating gas cloud collisions with dissipation of energy is highly enhanced.

If the formation of disks in galaxies is a rather recent phenomena occurring at a redshift of 2–5 (see, for instance, Koo 1986), then we may argue that as the density contrast is $\delta\rho/\rho \simeq 1$ in scale of some Mpc, it may be possible to speculate on a connection between galaxy morphology and large-scale structure through the dissipation mechanism depicted above.

1 On a fellowship from the Consejo de Investigaciones Científicas y Tecnológicas de la Provincia de Córdoba, Argentina.

Indeed, if disks formed recently, the conditions of the gas in different environments might have been sufficiently diverse, and we might think that the gas clouds of our models could form only in those regions where the temperature and therefore the density were low enough. In the case of a high-density region, the fragmentation of the gaseous medium might have been inhibited, generating a suitable condition for the genesis of the morphology-density relation that we observe today.

In the models, we assume that effective collisions between two gas clouds occur if a certain fraction of the clouds is overlapped, i.e., if the clouds fulfill the relative distance criteria $|r_i - r_j| < d_{\min}$. These effective collisions consist of a coalescence of two colliding clouds into one in the local rest frame. However, if a gas cloud has suffered several collisions, it might be in conditions of fragmentation and star formation. At this time, we consider that after $n_c = n_{c_{\max}}$ collisions the encounter with other cloud is no longer inelastic (the clouds do not merge any more). This cutoff in the permitted number of effective collisions is a parameter related to the efficiency of star formation. We assume that the star formation rate induced by collisions is suppressed after $n_{c_{\max}}$ collisions; the remaining gas is not in conditions of fragmentation, because it has been largely heated after several encounters. Therefore, the cloud will not merge with other similar clouds in a positive energy encounter. In this case, the reheating of the clouds would inhibit star formation, or at least severely reduce the efficiency of gaseous cooling (Bond, Szalay, and Silk 1983).

The physics of the gas in the process of galaxy formation is very complicated, and we are assuming here that the only mechanism for dissipation of energy is by means of cloud-cloud collisions. Also, we do not take into account energy release mechanisms such as supernovae explosions that would be present in a protostar cluster. We are therefore neglecting radial accelerations due to supernovae and any other source of energy dissipation by the clouds of gas in the absence of collisions. However, we expect that this simple mechanism might have occurred, and this gives us an insight into the consequences of the phenomena of dissipation.

The distribution of gas clouds is represented by an autogravitating system of softened particles in a potential well following a Schuster distribution with scale length a in the range 10–40 kpc (halo):

$$\rho_{\rm halo} \propto (r^2 + a^2)^{-5/2} .$$

The total fraction of mass in the halo with respect to the mass in clouds has been varied in the experiments from 1–50.

The initial spatial distribution of the clouds was taken as a uniform sphere of radius 100 kpc (Eggen, Lynden-Bell, and Sandage 1962), and the velocities were set as a solid-body rotation corresponding to a total λ parameter of $\simeq 0.07$, the mean value expected in a hierarchical clustering scenario from tidal torques (see the next section). We have assumed that the halo is initially rotating with the same angular momentum per unit mass as the clouds. We have adopted an initially solid body rotation for reasons of simplicity; in the absence of dissipation, an increase of rotational velocity as a function of radius is expected in a hierarchical clustering due to the torquing of the neighboring matter distribution (nevertheless, note that the initial amount of angular momentum is not dynamically significant). We have also tested other values of the initial spin parameter ($\lambda = 0.01$, 0.10, 0.12). Other experiments had the same initial velocity distribution, but the spatial distribution was an ellipsoid of semiaxes (100, 100, 80 kpc), with the minor axis parallel to the initial angular momentum vector. Some experiments were initially centrally concentrated, the initial density following an r^{-2} law, perhaps a more relastic situation at maximal expansion, where the inner shells have already collapsed and relaxed.

Soon after the collapse, the subsystem with high values of effective collisions n_c settles in a strongly flattened structure where rotation is dynamically dominant; this subsystem has undergone a large reduction of the original size. On the other hand, the subsystem consisting of those particles that have experienced no effective collisions is extended, roughly spherical and with a small ratio of rotational to total kinetic energy.

We analyzed experiment HALO3 with $d_{\min} = 0$ (nondissipative) and identical conditions as experiments HALO1 and 2 in order to check the dissipational scheme. Comparing these simulations, we found that the dynamical properties of clouds with $n_c = 0$ in these two latter were very similar to those of HALO3. This implies that the dynamics of noncolliding clouds is roughly independent of the presence of the high n_c subsystem (see § VI). Models where no massive halo was included were also analyzed; the results of these simulations (not shown in this paper) are characterized by a decrease in the ability of the coalescence mechanism to produce a highly flattened rotational supported system. The cause of this behavior is due to the relevance of two-body effects in the collisions. Thus the presence of a dominant halo might be an important fact in the formation of flattened glaaxies. Note, however, that in a realistic situation, the number of gas clouds is two orders of magnitude greater than in our simulations and in this case even without a dominant halo, two-body effects might be unimportant. It would be very interesting to follow the evolution of an experiment with $N \simeq 10^6$ particles, which is for the moment beyond our possibilities.

The total initial number of clouds was varied in the experiments between 1000 and 3000. For a ratio of halo to total mass in clouds (dissipative component) $M_H/M_D = 2$, the total mass of the system of clouds is $2.5 \times 10^{10}\ M_\odot$, giving individual cloud masses 0.8×10^7 to $2.5 \times 10^7\ M_\odot$, which is about two orders of magnitude larger than the Jeans mass at recombination ($M_J \simeq 10^5\ M_\odot$). Due to limitations in the number of particles, we were forced to work with the mentioned number of interacting clouds. Nevertheless, we did not find evidence of an N dependence of the results discussed below. The dominant halo is crucial in the lack of N dependence (two-body relaxation processes are unimportant).

The $n^{1/3}$ dependence of the mean free path should have been taken into account in adopting the cross section $d_{\min}$ and the particle softening ϵ. However, as is described in the next section, at fixed N and varying $d_{\min}$ a factor of 3, we found a similar dynamical behavior of the different n_c components.

III. INITIAL CONDITIONS

The density enhancement around the growing protogalaxy (potential well) is represented by a spherical $n = 5$ Schuster polytropic distribution, and the gas clouds are simulated by a distribution of softened equal mass particles. The halo is simulated by means of a very massive particle with large softening a. This way of representing the halo partially remedies the lack of response of an equivalent external field, because the halo can freely move in the simulations (White 1983). However, if the displacement of this "big particle" is large compared with the scale of the resulting distribution, we might worry that this representation is not good. We find that for $N \simeq 1000$ and $M_H/M_D > 2$, the displacements are unimportant.

We assume that initially, the system of clouds is at maximal expansion (no radial nor random kinetic energy), and that the gas is sufficiently cold to have clumped into discrete fragments represented by the particles. At maximal expansion, the system has acquired roughly the total amount of angular momentum by the tidal field from the neighboring mass distribution (see, for instance, Efstathiou and Jones 1979). At this stage, it is assumed that the angular momentum per unit mass is the same for the clouds as for the halo:

$$J_H/M_H = J_D/M_D = \sum J_{vi}/\sum m_{vi} , \quad (1)$$

where m_{vi}, J_{vi} are the virial mass and virial angular momentum of particle i, J_H and M_H are the total angular momentum and total mass of the halo, and J_D and M_D are the total angular momentum and total mass of the clouds (dissipative component).

Then we may compute the velocities for the clouds, taking into account that individual virial masses for the clouds are:

$$m_{vi} = \sum f_i v^2{}_i/\sum \sum f_i f_j r_{ij}{}^2/(r^2{}_{ij} + \epsilon_{ij}^2)^{3/2} . \quad (2)$$

We assume that initially the halo is in virial equilibrium, so

$$2T_H = U_H = 0.15GM_H/a , \quad (3)$$

where T_H and U_H are the kinetic and potential energy of the halo, respectively.

The resulting total virial spin parameter is:

$$\lambda_v = |\sum f_i r_i \cdot v_i| \cdot$$
$$\{[\sum \sum f_i f_j (r_{ij}{}^2 + 2\epsilon_{ij}{}^2)/(r_{ij}{}^2 + \epsilon_{ij}{}^2)^{3/2}]^{1/2}\} \cdot$$
$$\{[\sum \sum f_i f_j r_{ij}{}^2/(r_{ij}{}^2 + \epsilon_{ij}{}^2)^{3/2}]^{1/2}/(2 \sum f_i v_i^2)^{1/2}\} ,$$

where $f_i = m_i/M_D = m_{vi}/M_{vD}$, and the sums extend over all particles.

There are two possible values for the initial angular velocities consistent with a given value of the spin parameter λ: $\omega_1 < w_2$; ω_2 implies a large ratio of kinetic to potential energy $K/W \geq 1$, which is in contradiction with the assumed state of maximal expansion (minimum of kinetic energy). So, in all experiments, the smaller ω_1 is adopted.

The assumption that initially the angular momentum per unit mass is the same for the halo and the gas clouds is a standard hypothesis, based on the fact that the tidal field has acted in a similar way on both distributions (see, for instance, Fall 1983).

IV. DISSIPATION SCHEME

Dissipation is taken into account through cloud-cloud collisions. Whenever two particles of mass m_i and m_j collide, satisfying the relative distance criteria $|r_i - r_j| < d_{\min}$ (effective collision) independent of their relative velocities, they will be merged in a unique particle of mass $m_i + m_j$ and the same softening parameter ϵ, located in the center of mass frame.

We have adopted different criteria for $d_{\min}$ (see Table 1) and analyzed the resulting configurations for different values. We find that $d_{\min}$ is a sensitive parameter in the effectiveness of the collisions. Nevertheless, the equilibrium properties of the clouds after several effective collisions are almost independent of $d_{\min}$. In order to avoid the extreme situations, namely (*a*) initially (at maximal expansion) most of the collisions occur and (*b*) only a negligible fraction of the particles coalesce after the collapse, we adopted $d_{\min}$ in the range 0.0030–0.0100. Due to the independence of the equilibrium properties of the system of clouds in a given range of n_c on $d_{\min}$, this parameter turned out to be a computation effectiveness parameter, more than a fundamental ingredient of the models.

The adopted cross sections $d_{\min}$ in the experiments are a fraction 0.1–0.5 of the softening parameters of the particles representing the gas clouds, and they are a very small fraction of the initial mean interparticle distance (approximately 0.01). The fact that two clouds merge only by a distance criteria will be discussed in later sections. We could imagine that the encounter is largely radiative to keep the temperature constant during the collision. The cross section, independent of the relative velocity, requires that the typical encounter velocity does not largely exceed the rms velocity of the gas in the clouds.

Another important parameter in the experiments is the limit $n_{c_{\max}}$ in the number of effective collisions n_c of the clouds. We tested several experiments and found that for $n_c < 5$, energy dissipation is not sufficient for generating flattened rotational supported structures. For these subsystems, the spin parameter λ is not very different from those with $n_c = 0$ (particles that had no effective collisions). Therefore, if we set $n_{c_{\max}} > 20$, many clouds will have $n_c > 5$ and exhibit the desired dynamical properties.

In the paper of Bluementhal *et al.* (1986), a so-called fat baryon formed at the center of the system. This happened because in their experiments there was not a threshold for dissipation ($n_{c_{\max}}$ in our models). Physically, $n_{c_{\max}}$ is related to the gas physics and star formation process. If after several collisions a cloud has transformed a considerable fraction of mass into stars, a new collision with a similar cloud will result in the coalescence of the small fraction of gas remaining in the clouds, while the star components will interpenetrate each other with no energy dissipation and continue with their trajectories. We are neglecting here a possible merge of the stellar components; this is partially justified in the experiments because most of the two-body orbit energies are $E \gg 0$, and we know in this case that a collision will not produce a merger (see Navarro and Mosconi 1989, and references therein).

V. ANALYSIS OF THE EXPERIMENTS

We followed numerically the dynamical evolution of the system by means of the N-body 2 code using the Ahmad Cohen neighbor scheme, kindly given to us by Sverre Aarseth. A merging routine was included in the code in order to search for collision candidates in the neighbor sphere. For this type of simulation, this code is very efficient, and we found no need to use other codes (for instance, a tree code, which would have been more efficient in a standard N-body simulation with $N > 1000$). Typical CPU times for each simulation were of 20–50 hr in the μ-VaxII of the Observatorio Astronómico de Córdoba.

In all simulations, we have adopted $M_H + M_D = 1 \equiv 10^{11}$ $M_\odot$, $G = 1$, and the units of distance and velocity, 100 kpc and 65 km s^{-1}, resulting a time unit of 1.5×10^9 yr.

We have run several experiments with different model parameters and initial conditions. They are summarized in Table 1. In the experiments, we tried to explore both computational and model parameter dependence of the resulting largely dissipative components.

a) *Analysis*

The time evolution of global parameters of the system are shown in Figure 1 for experiment HALO23. It is seen a rapid

TABLE 1

MODEL PARAMETERS AND INITIAL CONDITIONS

Experiment	N	λ	a	f	M_H/M_D	d_{min}	$n_{c_{max}}$	Initial Particle Distribution
HALO1	1000	0.07	0.2	0.8	2	0.0200	Infinite	Uniform
HALO2	1000	0.07	0.2	0.8	2	0.0050	Infinite	Uniform
HALO3	1000	0.07	0.2	0.8	2	0.0000	Nondissipative	Uniform
HALO4	1000	0.07	0.2	0.8	10	0.0050	Infinite	Uniform
HALO5	3000	0.07	0.2	0.8	30	0.0035	20	Uniform
HALO6	3000	0.07	0.2	0.8	30	0.0035	Infinite	Uniform
HALO7	1000	0.07	0.2	0.8	10	0.0035	20	Uniform
HALO8	1000	0.07	0.2	1.0	10	0.0035	20	Uniform
HALO9	2000	0.07	0.2	1.0	20	0.0035	20	Uniform
HALO10	1000	0.07	0.1	1.0	10	0.0035	50	Uniform
HALO11	1000	0.07	0.2	1.0	5	0.0035	50	Uniform
HALO12	1000	0.07	0.2	1.0	5	0.0050	50	Uniform
HALO13	1000	0.01	0.2	1.0	10	0.0035	20	Uniform
HALO14	1000	0.10	0.2	1.0	10	0.0035	20	Uniform
HALO15	1000	0.07	0.2	1.0	10	0.0100	20	Uniform
HALO16	1000	0.07	0.2	1.0	5	0.0100	30	Uniform
HALO17	1000	0.07	0.2	1.0	2	0.0050	30	Uniform
HALO18	1000	0.07	0.2	1.0	2	0.0100	30	Uniform
HALO19	1000	0.12	0.2	1.0	2	0.0100	30	Uniform
HALO20	1000	0.07	0.2	1.0	1	0.0100	20	Uniform
HALO21	1000	0.07	0.2	1.0	50	0.0050	30	Uniform
HALO22	1000	0.07	0.2	1.0	50	0.0100	30	Uniform
HALO23	1000	0.07	0.2	1.0	10	0.0050	30	Inverse square law
HALO24	1000	0.07	0.2	1.0	5	0.0050	30	Inverse square law
HALO25	1000	0.07	0.2	1.0	20	0.0050	30	Uniform
HALO26	1000	0.07	0.2	1.0	50	0.0050	30	Inverse square law
HALO27	1000	0.07	0.2	1.0	20	0.0050	30	Inverse square law
HALO28	1000	0.07	0.4	1.0	10	0.0050	30	Inverse square law
HALO29	1000	0.07	0.4	1.0	50	0.0050	30	Inverse square law

NOTE.—a is the softening parameter of the halo, and f represents the initial flattening of the distribution.

relaxation in the system for the different components defined by a range in n_c. One can see here that there is a large collapse factor for large n_c; $n_c = 0$ has an equilibrium gravitational radius roughly $\frac{2}{3}$ of the initial, while the $n_c > 10$ component has reduced this radius a factor of 7. Also for this component, one can visualize the dynamical importance of rotation with respect to the $n_c = 0$ subsystem. In the postcollapse quasi-equilibrium period, the virial spin parameter computed from summing separately for different n_c ranges has reached stationary values: $\lambda_{n_c=0} \simeq 0.07$ and $\lambda_{n_c>10} \simeq 0.26$. This figure also shows the angular momentum per unit mass J/M. It is seen here that there is a net transfer of angular momentum per unit mass from the inner $n_c > 10$ component to the outer $n_c = 0$ (see White *et al.* 1987; Quinn and Zurek 1988; Zurek *et al.* 1988). Nevertheless, this is not very important dynamically, since there is not a large drag of the $n_c = 0$ component due to the high n_c rotating subsystem.

Figure 2 shows the time evolution of the ratio of rotational versus total kinetic energy T_{rot}/T_{tot} of experiment HALO23 for $n_c = 0$, and $n_c > 5$. The different relative amounts of T_{rot}/T_{tot} of the two components are evident from the figure. We have found a smooth transition toward rotational equilibrium as one approaches higher values of n_c in all experiments.

We show in Figure 3 several superposed snapshots of two-dimensional projections ($x - y$, $x - z$, $y - z$) of the components $n_c = 0$ and $n_c > 10$ in the quasi-stationary period 3×10^9 to 10^{10} yr in the experiment HALO19. One can see in the figure that there is a remarkable shrink and a strong flattening (6:1) of the component $n_c > 10$; the z-direction, parallel to the angular momentum vector, is devoid of particles in the large n_c subsystem. Note that Figure 3*b* shows only the inner 26 kpc of the distribution of the $n_c = 0$ component, which is far more extended, as seen in Figure 3*c*.

Depending mainly on d_{min}, the fraction of mass that settles in a flattened configuration varies largely in the models. For instance, experiment HALO14 grew by only 10% of the total mass in clouds with $n_c > 10$ after 10^{10} yr while at the same time, 90% of the total mass in clouds was in that component in HALO19. This fact is related to the efficiency of the coalescence process. For large values of d_{min}, there is a large efficiency in that process and a large number of clouds suffer several collisions. Note also that these two experiments as well as most of the simulations had no initial flattening nor anisotropies in the velocity distribution other than the imposed solid-body rotation.

It is important to note that there is not a significative evolution between 2 and 10 collapse times for different range in n_c. This is evident from the evolution of global parameters shown in Figure 1 for $n_c = 0$ and $n_c > 10$. This is the argument for superposing the distributions of a given range in n_c at different times after the collapse in Figures 3 and 4 and points toward a state of quasi-equilibrium for each component. Also we found that the three-dimensional distributions are very stable during this period of time.

Some experiments show a very definite ring structure. In Figure 4*a* are shown the $x - y$, $x - z$, and $y - z$ projections of experiment HALO21, with $M_H/M_D = 10$. This ring structure is produced by the lack of a strong mass concentration in the central region. This behavior is due to the fact that the Schuster potential is flat inside the effective radius a. As the relative

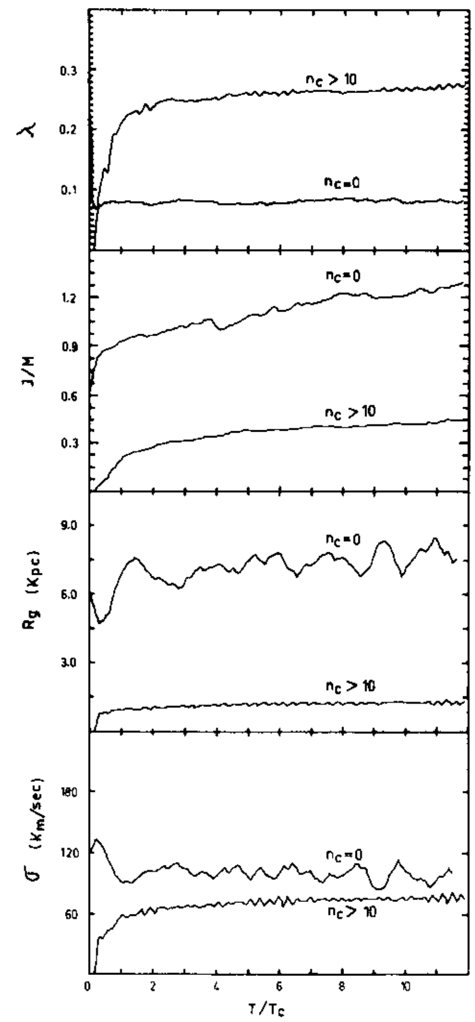

FIG. 1.—Time evolution of global parameters of experiment HALO23 for $n_c = 0$ and $n_c > 10$, in units of the collapse time T_c. (*top to bottom*): Virial spin parameter defined in § III, Angular momentum per unit mass J/M, gravitational radius $R_0 = GM^2/|W|$, where M and $|W|$ are the total mass and potential energy computed only for the ranges in n_c indicated in the figure, and total velocity dispersion for the two components.

mass of the halo is reduced, the ring tends to transform in a disk. This is visualized in Figure 4*b* for experiment HALO17, where the mass ratio is $M_H/M_D = 2$.

This tendency to fill the central region is seen in all experiments where many particles settle after the collapse in the center, and contribute sensible to the gravitational field of the halo at radii $r < a$. Experiments HALO23, 24, 26, 27, 28, 29 show a disklike structure instead of a ring for high n_c after the collapse. These simulations had an initial concentration given by a r^{-2} density law. In spite of the presence of a dominant halo ($M_H/M_D = 5$, 10, 20, 50), these models develop a central core long before the collapse of the outer shells. This core might be associated with the bulge of disk galaxies which, in current models of galaxy formation, assembled before the disks (see Fig. 4*c*).

The size of the ring is ruled by the effective radius a of the dominant Schuster distribution. In model HALO10, we varied a by a factor of 2 from model HALO8, and we found that a similar ring was formed of about half the size.

It is remarkable that in the experiments that have a roughly stationary ring structure for the high n_c component, the very massive particles (when permitted by $n_{c_{max}}$) are also in the ring and not in the central region of the system, as one could first imagine. This says that the dissipation is indeed an effective mechanism for enhancing the relevance of rotation and that dynamical friction within the particles due to the mass spectrum originated by the dissipational mechanism is not important because of the presence of the halo.

We found no important dynamical differences in a given component $n_{c_1} < n_c < n_{c_2}$ at different times. This is an interesting property of the model: dissipation in the collapse episode acts in an equivalent way as dissipation in the postcollapse slowly accreting phase. This fact gives support to the adopted cross section criteria independent of the encounter velocity, since the typical relative velocities in the collapse are much greater than those in the accreting phase, and nevertheless the dynamical properties are similar.

We have explored in all the models the viscous nature of the numerical simulations and have found that, with the number of particles $\simeq 10^3$ and d_{min} in the range 0.0035–0.01, the ratio of the mean free path between cloud collisions and the system radius (Gott and Thuan 1976) is

$$\lambda/R \simeq 1\text{–}20 .$$

Thus, our systems involve a viscous dissipative energy mechanism due to the parameters adopted. According to

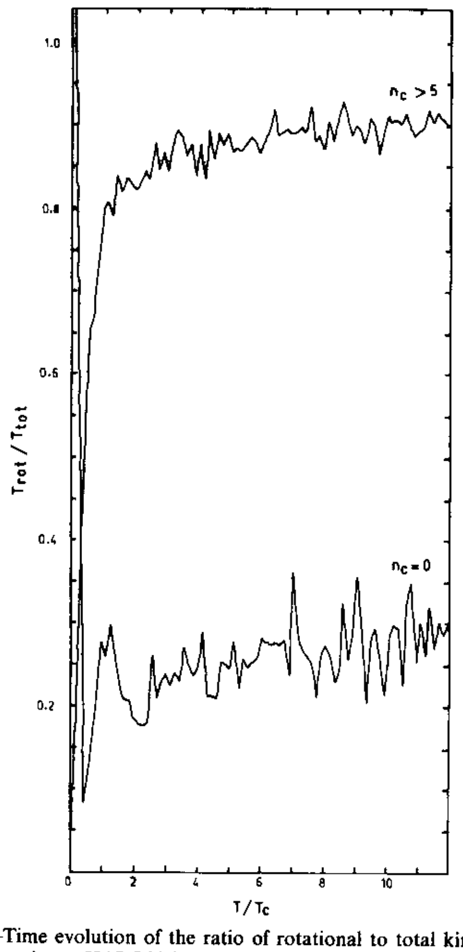

FIG. 2.—Time evolution of the ratio of rotational to total kinetic energy T_{rot}/T_{tot} in experiment HALO23 for $n_c = 0$, and $n_c > 5$, in units of T_c.

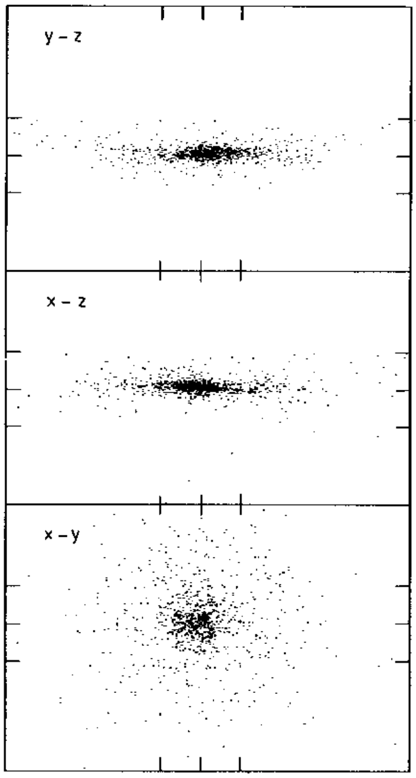

FIG. 3*a*

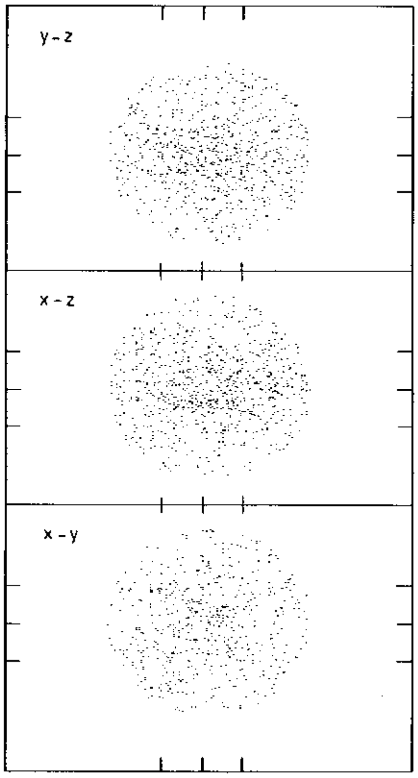

FIG. 3*c*

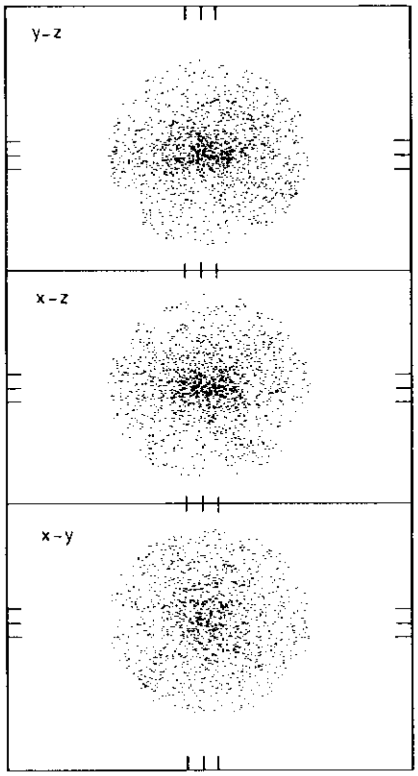

FIG. 3*b*

FIG. 3.—Projected views $x - y$, $x - z$, $y - z$ of experiment HALO19 in the stationary period $3 \times 10^9 < t < 3 \times 10^{10}$ yr ($2T_c$–$20T_c$); each tic corresponds to 10 kpc. (*a*) Component $n_c > 10$. (*b*) Component $n_c = 0$ ($R < 25$ kpc). (*c*) Component $n_c = 0$ ($R < 80$ kpc).

Larson (1975), viscosity might be important to avoid the flattening of the dissipative component; however, we find that there is a strong flattening despite the importance of viscosity. We believe it would be interesting to study in more detail the relevance of viscosity in dissipative systems.

Figure 5 shows the time evolution of the total number of particles and its relative variation in experiment HALO25. The reduction in the total number of clouds due to the coalescence mechanism is a continuous and asymptotic process. We notice a large variation in the number of particles $\Delta N/N$ in the collapse, and that after two collapse times, the variations in the number of particles $\Delta N/N$, are only a few percent. In most experiments, we found that the number of particles in the high n_c component only begins to grow long after the collapse, while there are soon many particles with moderate n_c.

Rotation curves of spiral galaxies are a puzzle for both the mass distribution and the dynamics of the gas and the stars. We have computed the mean rotation curves (binned in distance R to the z-axis and averaged over several times in the quasi-equilibrium postcollapse regime) for different n_c in all experiments. Figure 6 shows the mean rotation curve of model HALO17 for $n_c = 0$ and $n_c > 10$. Note from the figure that beyond 10 kpc, the nondissipative $n_c = 0$ component has a mean rotation velocity $\simeq 20$ km s^{-1}, much below the 80 km s^{-1} of the $n_c > 10$ component at the same radii. Due to the presence of the massive halo, the rotation curve of this component (more than 50% of the total mass in clouds) is roughly flat, in contrast with the $n_c = 0$ subsystem, which exhibits a large decay after 5 kpc. This is a typical behavior of the systems in the simulations, and the interpretation is straightforward: the rather flat rotational equilibrium velocity, $v = GM(\leq r)/r$ is approached only by the highly dissipative component. It is

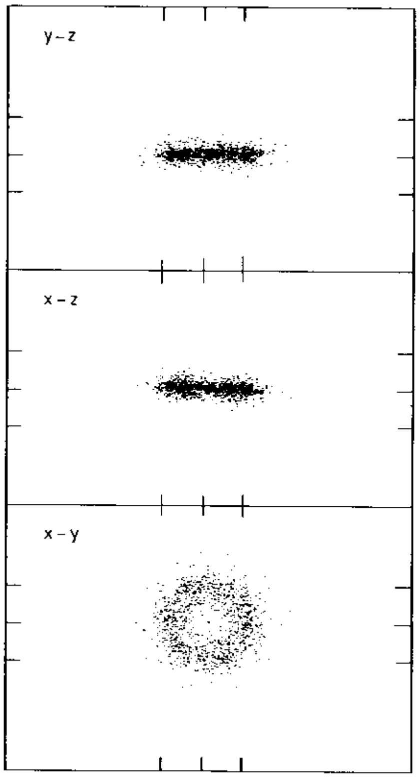

FIG. 4*a*

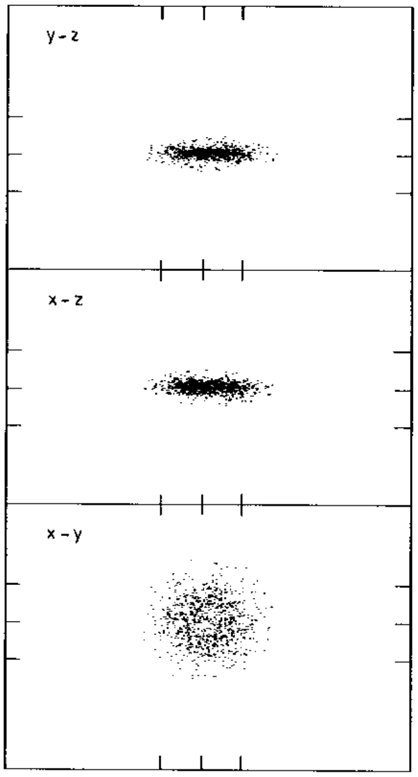

FIG. 4*c*

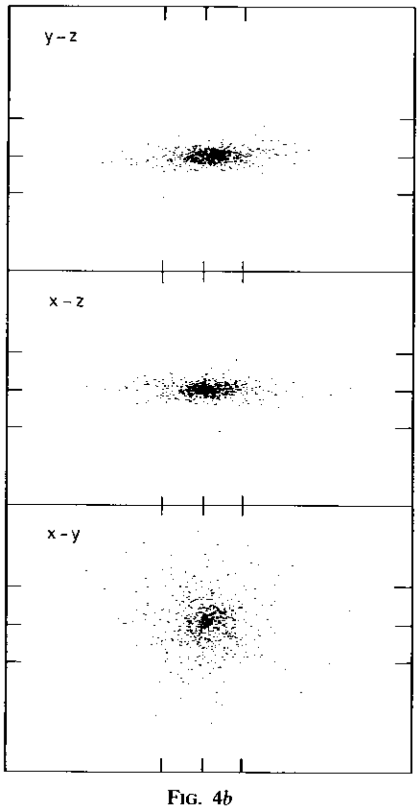

FIG. 4*b*

FIG. 4.—Projected views of the highly dissipative component $n_c > 10$ in the stationary period $3 \times 10^9 < t < 3 \times 10^{10}$ yr ($2T_c$–$20T_c$); each tic corresponds to 10 kpc. (*a*) Experiment HALO21 ($M_H/M_D = 50$). (*b*) Experiment HALO17 ($M_H/M_c = 2$). (*c*) Experiment HALO26 ($M_H/M_D = 50$, initial density r^{-2} law).

important to notice that the scatter of the $n_c = 0$ rotation curve is far greater than in the $n_c > 10$, which is related to the larger radial motions in the component $n_c = 0$.

The z-velocity dispersion is also strongly suppressed in the high n_c component. In Figure 7 we can see this effect for experiment HALO25 in the $\sigma_z - R$ diagram. We notice here that there is also a decreasing trend in σ_z with R for $n_c > 10$ (but in a much reduced scale compared with the $n_c = 0$ component) and the absence of particles in the central region; notice that this model develops a ring (see Table 1).

In order to analyze the flattening of the cloud distributions of different n_c, we have computed the moments of inertia J_x, J_y, and J_z for all experiments with $\lambda = 0.07$ in the postcollapse regime. A convenient flattening parameter $f^2 = 2J_z/(J_x + J_y)$ was derived for different n_c in all experiments. Figure 8 shows the dependence of f with n_c. It can be seen in the figure the trend of increasing flattening with increasing number of collisions. It is important to notice that although there is a quite large scattering among different experiments for a given n_c, a transition occurs for $n_c \simeq 5$ for all of them. This is an interesting feature, because model parameters were largely varied in the simulations.

It should be noted that the dissipational scheme would not stand if, for instance, $n_c > 100$ collisions were needed in order to provide enough flattening and rotation. The fact that in all experiments only a moderate number of collisions is sufficient to provide those dynamical properties is indeed encouraging.

HALO13 with initial $\lambda = 0.01$ did not develop a strongly flattened structure for the high dissipative component as in experiment with initial $\lambda = 0.07$. This obvious dependence of the equilibrium configuration on the initial spin parameter might be thought of as a possible explanation for the origin of the observational morphology-density relation.

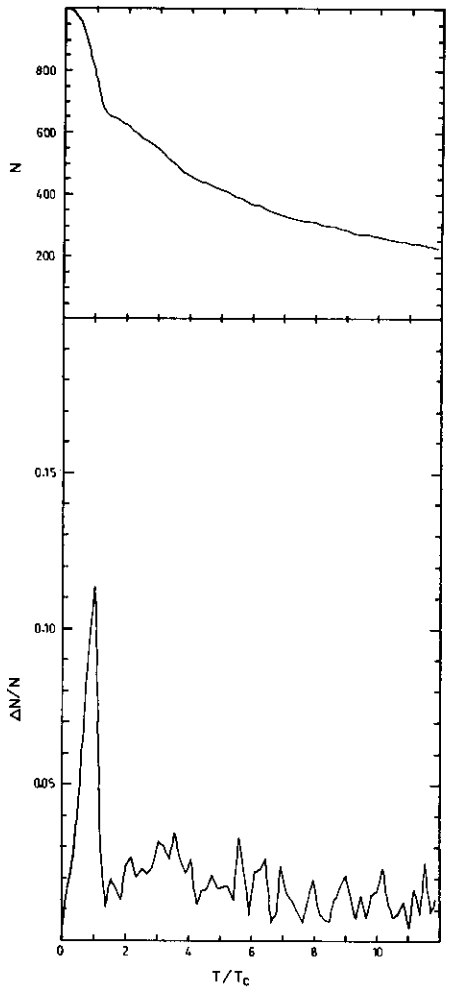

FIG. 5.—Time evolution of the total number of clouds N and the relative variations $\Delta N/N$ for experiment HALO25, in units of T_c.

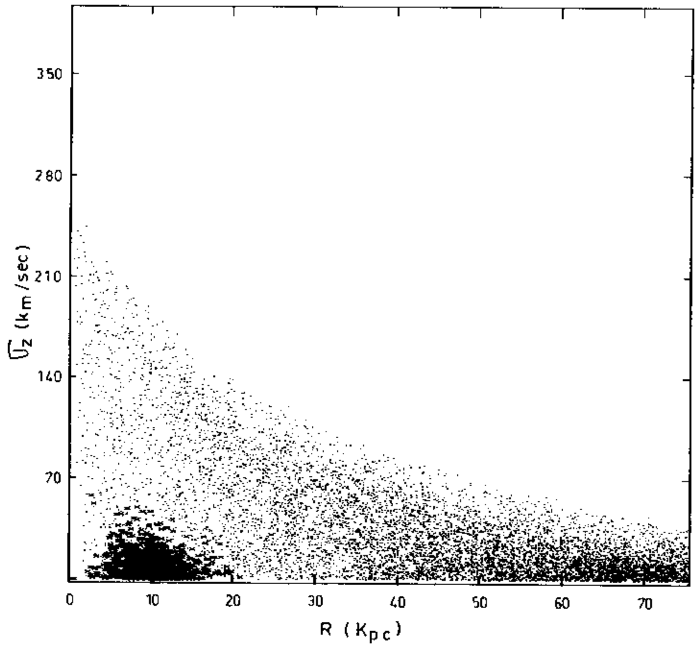

FIG. 7.—z-velocity dispersion vs. radius R for experiment HALO25 in the period $3 \times 10^9 < t < 10^{10}$ yr ($2T_c$–$20T_c$). Dots correspond to the component $n = 0$, crosses correspond to $n_c > 10$.

One should keep in mind, however, that although there is an increasing trend of initial mean λ with decreasing local density, dispersions around the mean value are very large, and it might be difficult to account for the morphology-density relation using only this argument. However, the gas might not be in conditions of fragmentation in high-density regions, and therefore only a small fraction of the gas might be able to undertake the process described in our models.

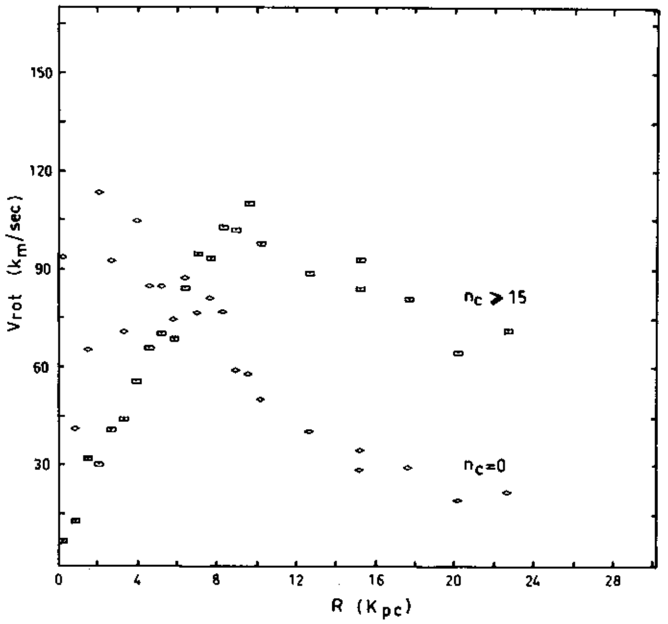

FIG. 6.—Rotation curves for experiment HALO17. Different symbols correspond to the average rotational velocity computed for $n_c = 0$ and $n_c > 15$ between $2T_c$ and $20T_c$.

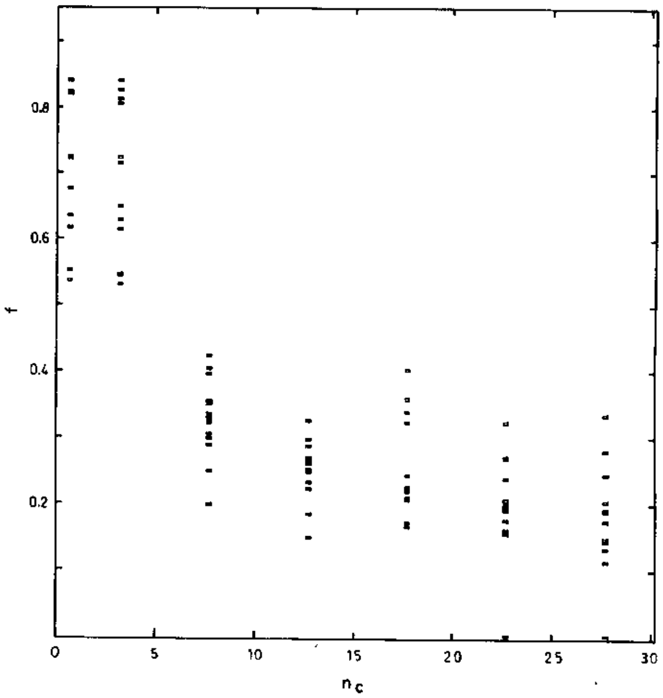

FIG. 8.—Flattening parameter $f = [2J_z/(J_x + J_y)]^{1/2}$ for all experiments with λ initial 0.07 averaged in the period $3 \times 10^9 < t < 10^{10}$ yr ($2T_c$–$20T_c$). The abscissa indicates the mean of the range in n_c taken in intervals of 5.

VI. DISCUSSION

The analysis of the experiments gives encouraging results pointing to a possible origin of a flattened rotating distribution, characteristic of most galaxies in the universe. It is indeed remarkable that the model works reasonably well for a wide range of global parameters, which suggests that dissipation of energy by means of inelastic collisions between gas clouds is very effective in setting a rotating disk or ring structure in a galactic potential well. These gas clouds can be related to the Jeans mass at recombination ($M_J \cong 10^5\ M_\odot$) and after $n_c = n_{c_{\max}}$ collisions, they would either be completely transformed into stars, or enormously heated; in both cases, the clouds no longer interact inelastically.

We conclude that the proposed mechanism of coalescence of gas clouds acts effectively as an amplifier of rotation versus random kinetic energy. We find that the subsystem with large n_c shrinks a factor of 5 into the center of the potential well in a time scale of the order of the collapse. This subsystem is characterized by an increasing flattening with increasing n_c, an increasing λ and $T_{\rm rot}/T_{\rm tot}$ with n_c, z-velocity dispersion σ_z decreasing with n_c. Typically $T_{\rm rot}/T_{\rm tot}$ rises from 0.1 initially to 0.9 for $n_c > 10$ and there is a strong suppression in σ_z, a factor of 3 between $n_c = 0$ and $n_c > 10$.

Of particular interest is the rearrangement of angular momentum in the simulations. We find a rise in the rotation curve at large radii for the highly dissipative component. For instance, in HALO17 at $R \cong 20$ kpc, the rotation velocity for $n_c > 10$ reaches 75 km s^{-1}, while for $n_c = 0$ this value is only 25 km s^{-1}.

We find that the formation of a ring depends on both the ratio of halo to total cloud mass M_H/M_D and the concentration of the initial distribution of clouds. We obtained rings instead of disks for large values of M_H/M_D (Five or greater), with an initial uniform distribution of clouds. However, if the initial distribution is radially concentrated (r^{-2} law), even for $M_H/M_D = 50$ no ring structure develops.

In principle, the dynamical dominance of the halo implies stability against bar formation (Ostriker and Peebles 1973; Efstathiou, Lake and Negroponte 1982). We have computed the parameter t defined by Ostriker and Peebles and have found it close to 0.1, which according to their criterion ($t \leq 0.14$) would indicate that the flat system remains stable to the formation of a bar. However, due to the limited dynamical range of the simulation, we cannot study properly the internal structure of the flat component (with typically only few tenths of particles).

We have explored the viscosity of the system of gas clouds in all the experiments according to the discussion of Gott and Thuan (1976). The ratio of the mean free path between cloud collisions to the system radius λ/R were found in the range 1–20. We see in the analysis of the experiments that despite the viscous nature of our simulations, there is a strong flattening in the dissipative component due to a rearrangement of angular momentum. If we recall previous discussions by Gott (1977) and Larson (1975), it is important to stress the fact that we find that viscosity in the dissipative component of a protogalaxy does not affect severely the growth of a flattened structure supported by rotation.

Regarding the question of the adopted criteria for the coalescence of two colliding gas clouds, which is independent of their relative velocity, we may argue that as we found that the dynamical properties of the highly dissipative component are the same during the collapse episode (high encounter velocities) and in the postcollapse regime (lower velocities), a velocity-dependent cross section would not severely change the main results obtained in the experiments. Thus, our crude model for taking into account dissipation of energy might give a good description of the phenomena.

It should be noted that in these experiments where the halo is very dominant ($M_H/M_D = 10$), there is no appreciable mass segregation by two-body relaxation.

This simple dissipative model might well be enlarged in order to take into account other important physical processes such as supernova explosions, gas heating, dynamical friction with the halo, and halo response to the collapse of the dissipative component. We think that the experiments presented here might help clarify the role of dissipation and angular momentum in galaxy formation. It might be noted once more that there is no need for a fine tuning of the model parameters in order to obtain reasonable dynamical properties of flattened galaxies. This virtue of the model encourages us to explore it in more detail.

Strong energy dissipation might have had an important role in the formation of galaxies of different morphologies. We plan to investigate the possible building of the galaxy sequence using this simple dissipative model.

We thank S. Aarseth for providing his N-body 2 code. We have benefited from discussions with J. Navarro and J. L. Sérsic. Useful comments from an anonymous referee are greatly appreciated. This work was partially supported by the Consejo de Investigaciones Cientificas y Técnicas de la Provincia de Córdoba, Argentina.

REFERENCES

Bahcall, J. N., Schmidt, M. A., and Soneira, R. M. 1982, *Ap. J.* (*Letters*), **258**, L23.
Blumenthal, G. R., Faber, S. M., Flores, R., and Primack, J. R. 1986, *Ap. J.*, **301**, 27.
Bond, J. R., Szalay, A., and Silk, J. 1983, in *Formation and Evolution of Galaxies and Large Scale Structures in the Universe*, ed. J. Audouze and J. Tranh Than Van (Dordrecht: Reidel), p. 101.
Caldwell, J. A. R., and Ostriker, J. P. 1982, *Ap. J.*, **251**, 61.
Carlberg, R. G. 1988*a*, *Ap. J.*, **324**, 664.
———. 1988*b*, *Ap. J.*, **332**, 26.
Davis, M., Efstathiou, G., Frenk, C., and White, S. D. M. 1985, *Ap. J.*, **292**, 361.
Efstathiou, G., and Jones, B. J. T. 1979, *M.N.R.A.S.*, **186**, 133.
Efstathiou, G., Lake, G., and Negroponte, J. 1982, *M.N.R.A.S.*, **199**, 1069.
Efstathiou, G., and Silk, J. 1983 in *Fund. Cosmic Phys.*, **9**, 1.
Eggen, D. J., Lynden-Bell, D., and Sandage, A. R. 1962, *Ap. J.*, **136**, 748.
Fall, S. M. 1983, in *Internal Kinematics and Dynamics of Galaxies*, ed. E. Athanassoula (Dordrecht: Reidel), p. 393.
Fall, S. M., and Efstathiou, G. 1980, *M.N.R.A.S.*, **193**, 189.
Gott, J. R. 1977, *Ann. Rev. Astr. Ap.*, **15**, 235.
Gott, J. R., and Thuan, T. X. 1976, *Ap. J.*, **204**, 649.
Hoffman, Y. 1988*a*, *Ap. J.*, **328**, 489.
———. 1988*b*, *Ap. J.*, **329**, 8.
Koo, D. C. 1986, in *Spectral Evolution of Galaxies*, ed. C. Chiosi and A. Renzini (Dordrecht: Reidel), p. 419.
Larson, R. B. 1974, *M.N.R.A.S.*, **166**, 585.
———. 1975, *M.N.R.A.S.*, **173**, 671.
———. 1976, *M.N.R.A.S.*, **176**, 31.
Navarro, J. F., and Mosconi, M. B. 1989, *Ap. J.*, **336**, 669.
Ostriker, J. P., and Peebles, P. J. E. 1973, *Ap. J.*, **186**, 467.
Peebles, P. J. E. 1969, *Ap. J.*, **155**, 393.
———. 1980, *The Large Scale Structure of the Universe* (Princeton: Princeton University Press).
Quinn, P. J., and Zurek, W. H. 1988, *Ap. J.*, **331**, 1.
Sandage, A., Freeman, K. C., and Stokes, N. R. 1970, *Ap. J.*, **160**, 831.
White, S. D. M. 1983, *Ap. J.*, **224**, 53.
White, S. D. M., Davis, M., Efstathiou, G., and Frenk, C. 1987, *Nature*, **330**, 45.
Zurek, W. H., Quinn, P. J., and Salmon, J. K. 1988, *Ap. J.*, **330**, 519.

Mario G. Abadi, Diego Garcia Lambas and Mirta B. Mosconi: Observatorio Astronómico, Laprida 854 5000 Córdoba, Argentina